Onset of synchronization in systems of globally coupled chaotic maps

Seung-Jong Baek[1,*] and Edward Ott[1,2]
[1]*Department of Electrical and Computer Engineering, Institute for Research in Electronics and Applied Physics, University of Maryland, College Park, Maryland 20742, USA*
[2]*Department of Physics, University of Maryland, College Park, Maryland 20742, USA*
(Received 2 March 2004; published 11 June 2004)

We study the transition to coherence of an ensemble of globally coupled chaotic maps allowing for ensembles of nonidentical maps and for noise. The transition coupling strength is determined from a kind of transfer function of the perturbation evolution. We present analytical results, and we test these results using numerical experiments for several large systems consisting of ensembles of many coupled maps. The later includes ensembles of identical noiseless maps, identical maps subject to noise, and ensembles of nonidentical maps. One of our examples suggests that the validity of the perturbation theory approach can be problematic for an ensemble of noiseless identical maps if the maps are nonhyperbolic. However, for such a case, noise and/or parameter spread seems to have a regularizing effect restoring the validity of perturbation theory.

DOI: 10.1103/PhysRevE.69.066210 PACS number(s): 05.45.Xt

I. INTRODUCTION

The onset of synchronization in large ensembles of globally coupled dynamical units is of interest in many fields [1]. Systems of this type have been examined in biology, where it is thought that rhythms are essential for maintaining life. In these biological situations rhythms are typically generated by a large number of cells or groups of cells, each one of which has a tendency to oscillate when isolated [2]. For example, heartbeats are stimulated by the sinoatrial (SA) node located on the right atrium, and the node consists of thousands of coupled pacemaker cells [2,3]. Each cell in the SA node has slightly different intrinsic frequency and, through electrical coupling, achieves a consensus as to when to fire [3]. Similar mechanisms are observed in networks of neurons [4], coupled neurons in the suprachiasmatic nucleus (the circadian center) [5], and suspensions of yeast cells [6]. Insects also exhibit synchronized behavior [7,8]. For example, it has been observed that a large number of certain types of fireflies flash on and off in unison. They apparently watch each other and adjust their flashing according to their neighbors. A small group of fireflies starts to flash synchronously, and the number of synchronized participants grows so that the whole swarm finally flashes in unison [7]. Swarms of crickets and grasshoppers also chirp in unison through a similar process [8]. Nonbiological examples of synchrony in large systems of globally coupled dynamical units occur in arrays of globally coupled chaotic electrochemical oscillators [9], semiconductor laser arrays [10], and Josephson junction arrays [11]. It is known that these systems experience a transition to a coherent state at some critical coupling strength. In particular, for low coupling the individual units essentially evolve independently (the "incoherent state"), but, as the coupling passes a critical value, the average over all units of an appropriate function of the unit state begins to take on a macroscopic value, signaling the onset of coherent, synchronous behavior of the system. The transition from incoherence to synchronization with increase of the coupling has been very extensively studied in the case where the uncoupled dynamics is *periodic* [1]. In particular, the well-studied "Kuramoto model" [1] considers many periodic oscillators whose uncoupled dynamics is described by the simple phase evolution equation, $d\theta^{(i)}(t)/dt=\omega^{(i)}$, for the phase $\theta^{(i)}$ of oscillator i, which has natural frequency $\omega^{(i)}$.

Very recently attempts to study the transition from incoherence to synchrony in the case where the individual units are *chaotic* systems of ordinary differential equation have been made [12–14]. Pikovsky *et al.* [12] numerically show that the transition to coherent behavior in a system of globally coupled nonidentical Rössler systems is due to the synchronization of phases of the individual units. They concentrate on the case that the individual systems have phase-coherent attractors and think of the transition as the synchronization transition in a system of coupled noisy limit-cycle oscillators. However, they do not develop a theory for the transition to synchrony. Sakaguchi [13] analyzes a large ensemble of globally coupled identical Rössler systems by assuming that, at the onset of coherence, the average motion of the ensemble is sinusoidal in time. Ott *et al.* [14] investigated the stability of the incoherent state for ensembles of globally coupled continuous-time dynamical systems using a perturbation method and analytic continuation. They numerically applied their theory to ensembles of globally coupled heterogeneous Lorenz systems with the parameters uniformly distributed in periodic, chaotic and mixed parameter regions. References [12–14] all treated ensembles of *noise-free* chaotic systems.

Concerning large systems of globally coupled chaotic *maps*, starting with the work of Kaneko [15], it has been known that, depending on parameters, these systems can exhibit either incoherent behavior, or coherent oscillatory (i.e., synchronized) behavior, and work has been done investigating the nature of these behaviors [15–18]. However, only one paper (Topaj *et al.* [19]) has so far given an analytical treatment of the transition from incoherence to coherence for a

*Electronic address: sjbaek@glue.umd.edu

large globally coupled map system. This paper, however, treats only the special case of identical $2x \bmod 2\pi$ maps.

In the present paper, we present a general method to determine the critical coupling strength and the frequency of oscillation at the onset of coherence in a system of globally coupled chaotic maps. Our analysis allows for arbitrary map functions, the inclusion of noise, and the treatment of ensembles that are heterogeneous (i.e., it is not required that all maps in the ensemble are the same). Also, we investigate techniques for numerical application of the analysis. Our analysis adapts to *discrete-time* (maps) the perturbation method which Ott *et al.* [14] applied to systems of globally coupled *continuous-time* dynamical systems. The goal is to relate the evolution of a perturbation of the individual uncoupled elements to the evolution of a perturbation of the globally coupled system. Thus, we represent the behavior of coupled systems in terms of the behavior of uncoupled elements.

The system model and the analysis of the system is presented in Sec. II. One-dimensional map examples employing and testing the analysis are given in Sec. III. One result of the numerical experiments in Sec. III C is that there is an apparent failure of the perturbation theory in a case of an ensemble of identical noiseless nonhyperbolic maps (in particular, the logistic map). However, the introduction of noise or of parameter spread appears to have a regularizing effect which seems to restore the validity of the perturbation theory approach. Section IV gives an example for an ensemble of two dimensional maps. The examples in Secs. III and IV contain ensembles of shifted Bernoulli maps, ensembles of modified Bernoulli maps in which a parameter of the map is uniformly distributed throughout an interval, ensembles of identical logistic maps, ensembles of identical noisy logistic maps, ensembles of noiseless logistic maps with a uniform distribution of the map parameter in an interval, and ensembles of cat maps.

II. SYSTEM MODEL AND ANALYSIS

A. System model

In this section we study systems of globally coupled, chaotic, one-dimensional maps similar to the system studied in Ref. [19]. (The generalization to higher-dimensional maps is made in Sec. IV). In our theory, we assume that there is a mixing chaotic attractor so that almost every orbit of the uncoupled system yields the same long-time statistical behavior. The general form of the system we consider is

$$x_{n+1}^{(i)} = f(x_n^{(i)}, \mu_i) + w_n^{(i)} + kg(x_n^{(i)})[\langle q(x_n)\rangle - \langle q(x)\rangle_*], \quad i = 1, \ldots, N$$

$$\langle q(x_n)\rangle = \frac{1}{N}\sum_{i=1}^{N} q(x_n^{(i)}). \tag{1}$$

The quantity $w_n^{(i)}$ in Eqs. (1) is a random noise where $E[w_n^{(i)}]=0$, $E[w_n^{(i)}w_k^{(j)}]=\sigma^2\delta_{nk}\delta_{ij}$, $E[\cdot]$ denotes the expectation value, σ^2 is the variance of the noise, and for each n and i the $w_n^{(i)}$ are identically distributed. Moreover, we assume that x_n and w_n are independent. We note that additive noise makes the time averaged orbit probability distribution function of an uncoupled map smooth so that the distribution has no singularities [20], and noise may also eliminate small periodic windows within the chaotic parameter region. The maps $f(x,\mu_i)$ are assumed to arise from a one parameter family with parameter μ_i, and we assume that the μ_i are distributed in some specified manner. For example, in our examples (Sec. III) we will consider the case where the μ_i are distributed uniformly in an interval, and also the case of identical maps where all the μ_i are the same ($\mu_i=\mu$). Also in Eqs. (1), N is the ensemble size, k is the coupling coefficient, and the function $g(x)$ and $q(x)$ are assumed to be smooth and bounded. The symbol $\langle\cdot\rangle$ denotes the average over the ensemble (the average over i) at a fixed time n, and thus depends on n. The symbol $\langle\cdot\rangle_*$ denotes the infinite time mean for a typical orbit x_n of a noisy uncoupled map [$k=0$ in Eqs. (1), giving $x_{n+1}^{(i)}=f(x_n^{(i)},\mu_i)+w_n^{(i)}$] averaged over μ_i; thus $\langle\cdot\rangle_*$ is time independent. In the limit $N\to\infty$, a possible solution of Eqs. (1) is $\langle q(x_n)\rangle=\langle q(x)\rangle_*$, in which case the coupling has no effect. We refer to this solution as the "incoherent state." For large finite N, it is expected and numerically observed that for parameter values in the predicted $N\to\infty$ incoherent state $\langle q(x_n)\rangle$ executes small fluctuations of order $N^{-1/2}$ about $\langle q(x)\rangle_*$. As $|k|$ is increased, the incoherent state becomes unstable, and the mean field $a_n=\langle q(x_n)\rangle-\langle q(x)\rangle_*$ begins to have a macroscopic [i.e., $\mathcal{O}(N^0)$ rather than $\mathcal{O}(N^{-1/2})$] value. This transition typically occurs at some critical nonzero coupling coefficient k_c [14,19]. In fact there can be two critical k_c values, a positive one, at which coherence arises as k increases through the critical value, and a negative one at which coherence arises as k decreases through the critical value. It was shown for globally coupled, noiseless, continuous-time systems [14] that the transition from the incoherent state to the coherent state can be analyzed by a perturbation method. Here, we develop this perturbation method to analyze globally coupled, noisy, discrete-time systems (i.e., maps).

B. Stability analysis

We carry out the stability analysis for the system in the $N\to\infty$ limit. Thus, for the purposes of this analysis, given a function h, the symbol $\langle h(x)\rangle$ is now understood to mean

$$\langle h(x_n)\rangle = \lim_{N\to\infty}\frac{1}{N}\sum_{i=1}^{N} h(x_n^{(i)}).$$

We note that, while $N\to\infty$ in the analysis, our numerical experiments necessarily have finite N, and, as we will see in Secs. III and IV, the finiteness of N will have a profound effect for implementation of our theory in numerical examples, even though N will be very large in these examples. For compactness of notation, where it is unlikely to create confusion, we will henceforth drop the subscripts and superscripts i denoting the individual maps.

To perform the $N\to\infty$ stability analysis, we assume a small perturbation from the incoherent state and investigate

its stability. Let δ_n be a perturbation to x_n when there is no coupling, and let δx_n be the perturbation with coupling,

$$\delta_{n+1} = f'(x_n,\mu)\delta_n, \quad \delta_0 = 1, \tag{2}$$

$$\delta x_{n+1} = f'(x_n,\mu)\delta x_n + kg(x_n)\langle q'(x_n)\delta x_n\rangle. \tag{3}$$

[Note that, while the noise does not appear explicitly in Eqs. (2) and (3), its presence is still important since it influences the orbit x_n: $x_{n+1}^{(i)} = f(x_n^{(i)},\mu_i) + w_n^{(i)}$.] We are interested in how the mean field perturbation $\langle q'(x_n)\delta x_n\rangle$ develops from an initial perturbation $\langle q'(x_0)\delta x_0\rangle$. Setting

$$\delta x_n = z_n \delta_n, \tag{4}$$

in Eq. (3), and employing Eq. (2), we obtain

$$z_{n+1} - z_n = k\frac{g(x_n)}{\delta_{n+1}}\langle q'(x_n)\delta x_n\rangle,$$

recursive application of which yields

$$z_{n+1} = k\sum_{p=0}^{n}\frac{g(x_p)}{\delta_{p+1}}\langle q'(x_p)\delta x_p\rangle + z_0, \tag{5}$$

where $z_0 = \delta x_0$. Using the relation (4), we can obtain $\langle q'(x_n)\delta x_n\rangle$ from Eq. (5),

$$\langle q'(x_{n+1})\delta x_{n+1}\rangle = k\left\langle \sum_{p=0}^{n}\frac{\delta_{n+1}q'(x_{n+1})g(x_p)}{\delta_{p+1}}\langle q'(x_p)\delta x_p\rangle\right\rangle + \delta x_0\langle q'(x_{n+1})\delta_{n+1}\rangle. \tag{6}$$

Now, we assume exponential instability of the incoherent state so that the mean of the perturbation grows exponentially with n, $\langle q'(x_n)\delta x_n\rangle = \lambda^n\langle q'(x_0)\delta x_0\rangle$ with $|\lambda| > 1$. Then, we can rewrite Eq. (6) as

$$\lambda^{n+1} = k\left\langle \sum_{p=0}^{n}\frac{\delta_{n+1}q'(x_{n+1})g(x_p)}{\delta_{p+1}}\lambda^p\right\rangle + \frac{\delta x_0\langle q'(x_{n+1})\delta_{n+1}\rangle}{\langle q'(x_0)\delta x_0\rangle}.$$

Letting $n\to\infty$, assuming convergence of the summation, and setting $m = n-p$, we have

$$1 = \frac{k}{\lambda}\left\langle \sum_{m=0}^{\infty}\frac{P_m}{\lambda^m}\right\rangle \equiv kQ(\lambda), \tag{7}$$

where

$$P_m = \frac{\delta_{n+1}q'(x_{n+1})g(x_{n-m})}{\delta_{n-m+1}}.$$

The ratio $\delta_{n+1}/\delta_{n-m+1}$ is

$$\frac{\delta_{n+1}}{\delta_{n-m+1}} = f'(x_n,\mu)f'(x_{n-1},\mu)\cdots f'(x_{n-m+1},\mu). \tag{8}$$

For large m, this quantity increases exponentially with m as $\xi^m(x_0,\mu)$, where $\xi(x_0,\mu)$ is the Lyapunov number of the map $f(x,\mu)$ for the initial condition x_0. [For almost all x_0, $\xi(x_0,\mu)$ is the same number (i.e., what is usually referred as "the" Lyapunov number of the chaotic attractor), but there are special choices of x_0 (e.g., x_0 on an unstable periodic orbit) for which $\xi(x_0,\mu)$ takes on a different value.] For Eq. (7) to have meaning we require that the summation over m converges. This will be so if

$$|\lambda| > \xi_{\max} \equiv \sup_{x_0,\mu}\xi(x_0,\mu), \tag{9}$$

where x_0 is in the attractor basin and μ is in the range of parameter values used in the ensemble. If $|\lambda| < \xi(x_0,\mu)$, the m th term in the sum increases exponentially with m as $[\xi(x_0,\mu)/\lambda]^m$, and Eq. (7) is meaningless. For the case where λ satisfies Eq. (9), the exponential convergence of the summation implies that we can interchange the order of the average and the summation. Thus we obtain

$$1 = \frac{k}{\lambda}\sum_{m=0}^{\infty}\frac{Q_m}{\lambda^m} \equiv kQ(\lambda), \tag{10}$$

where $Q_m = \langle P_m\rangle$ or

$$Q_m = \left\langle \frac{\delta_{n+1}}{\delta_{n-m+1}}q'(x_{n+1})g(x_{n-m})\right\rangle. \tag{11}$$

Because we are dealing with chaotic situations (i.e., Lyapunov number greater than one), Eq. (9) implies that $Q(\lambda)$, given by Eq. (10), can, so far, only be used for λ sufficiently larger than one. We now argue that Eq. (10) can be expected to apply for $|\lambda| < 1$. This is crucial, since it is required in order to use the theory for studying the onset of coherence. We heuristically argue in Appendix A that the quantity Q_m can be expected to decrease exponentially with m for typical chaotic maps (a similar argument is presented in Ref. [14] for the case of continuous time systems). Assuming this to be the case, we have

$$|Q_m| < K\xi_*^{-m}, \tag{12}$$

where K and ξ_* are positive constants and $\xi_* < 1$. Thus the sum in Eq. (10) now converges for all $|\lambda| > \xi_*$. Hence, while Eq. (10) was derived for $|\lambda| > \xi_{\max}$, Eq. (12) implies that we can analytically continue $Q(\lambda)$ from the region $|\lambda| > \xi_{\max}$ to the region $\xi_{\max} \geqslant |\lambda| > \xi_* < 1$.

At the transition of the incoherent state to the coherent state (i.e., at $k = k_c$) the system is marginally stable so that $|\lambda| = 1$ or $\lambda = e^{i\omega}$ with ω real. Thus, $k_c Q(e^{i\omega}) = 1$. Taking the imaginary part of this equation, we obtain an equation for the frequency of oscillation ω at the transition

$$\mathrm{Im}\{Q(e^{i\omega})\} = 0. \tag{13}$$

After solving this equation for ω, we obtain the critical coupling strength,

$$k_c = Q(e^{i\omega})^{-1}. \tag{14}$$

In addition, expanding Eq. (10) about $k = k_c$ and $\lambda = e^{i\omega}$, we obtain the following result for λ near the transition

$$\lambda = e^{i\omega} + \frac{k_c - k}{k_c^2 Q'(e^{i\omega})} + \mathcal{O}\{(k_c - k)^2\},$$

where $Q'(\lambda) = dQ(\lambda)/d\lambda$.

III. EXAMPLES: ONE-DIMENSIONAL MAPS

A. An ensemble of shifted Bernoulli maps

Our first example is an ensemble of Bernoulli maps,

$$f(x_n^{(i)},\mu_i) = (2x_n^{(i)} + \mu_i) \bmod 2\pi, \quad i = 1, \ldots, N$$

$$g(x) = \sin 2x + \sin 4x,$$

$$q(x) = \cos x, \tag{15}$$

where μ_i is a shift which is in general different for each map i. Because of the simplicity of this example, $Q(\lambda)$ can be obtained analytically. After plugging Eqs. (15) into Eq. (11), and taking the noise w to be symmetrically distributed around $w=0$, we obtain

$$Q_n(\lambda) = -\frac{1}{\lambda}\sum_{p=0}^{n} \langle \sin x_{n+1}(\sin 2x_p + \sin 4x_p)\rangle \left(\frac{2}{\lambda}\right)^{n-p}$$

$$= -\frac{1}{2\lambda}\left(\langle \cos w_n\rangle\langle \cos \mu\rangle + \frac{2}{\lambda}\langle \cos 2w_{n-1}\rangle\langle \cos w_{n-2}\rangle \times \langle \cos 3\mu\rangle\right).$$

The second equality results from noting that, since $x_p \bmod 2\pi$ has a uniform density in $(0,2\pi)$, all terms in the summation are zero except for $p=n$ and $p=n-1$. In the above, if the ensemble of shift parameters $\{\mu_i\}$ is generated from a probability density $\rho(\mu)$, then

$$\langle \cos M\mu\rangle \equiv \int \rho(\mu)\cos(M\mu)d\mu.$$

Taking the noise w to be normally distributed, we obtain

$$Q(e^{i\omega}) = -\frac{1}{2}\left(\frac{e^{-\sigma^2/2}}{e^{i\omega}}\langle \cos \mu\rangle + \frac{2e^{-5\sigma^2/2}}{e^{2i\omega}}\langle \cos 3\mu\rangle\right).$$

For simplicity, in what follows we take $\rho(\mu)=\delta(\mu)$, so that $\langle \cos \mu\rangle = \langle \cos 3\mu\rangle = 1$, which with Eqs. (13) and (14), yields critical values

$$k_{c1} = e^{5\sigma^2/2}, \quad \omega_{c1} = \arccos\left(-\frac{e^{2\sigma^2}}{4}\right),$$

$$k_{c2} = -2(e^{-\sigma^2/2} + 2e^{-5\sigma^2/2})^{-1}, \quad \omega_{c2} = 0. \tag{16}$$

For $\sigma=0$, Eqs. (16) agree with the result of Ref. [19].

We present results of numerical experiments in Fig. 1 for the case that the system has no noise and the case that the system has normally distributed noise with $\sigma^2=0.16$. Without noise (i.e., $\sigma^2=0$), Eqs. (16) yield $k_{c1}^{(0)}=1$ at $\omega_{c1}^{(0)} = \arccos(-\frac{1}{4}) \approx 0.58\pi$ and $k_{c2}^{(0)}=-2/3$ at $\omega_{c2}^{(0)}=0$. With $\sigma^2=0.16$, Eqs. (16) yield the critical values $k_{c1}\approx 1.49$ at $\omega_{c1}\approx 0.61\pi$ and $k_{c2}\approx -0.88$ at $\omega_{c2}=0$. In Fig. 1(a), $\langle a^2\rangle$ is the time average of the square of the mean field $a_n = \langle q(x_n)\rangle - \langle q(x)\rangle_*$ and this average is computed over 1000 iterations in time. We see that the mean field starts to have macroscopic

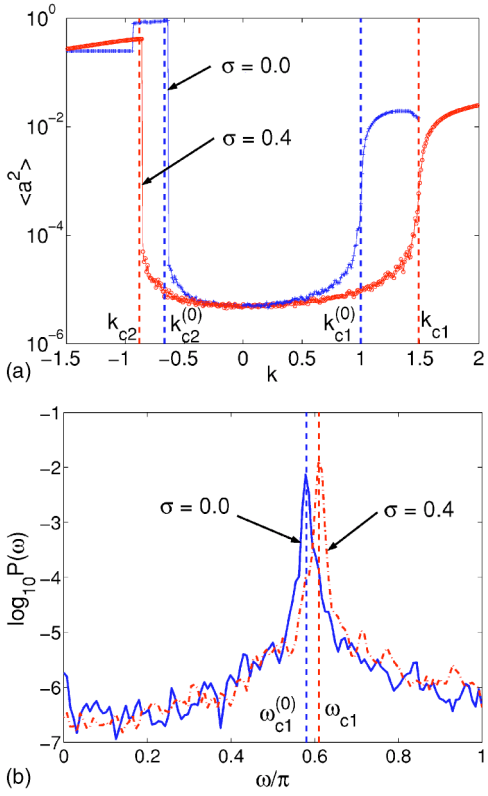

FIG. 1. Results for an ensemble of $N=10^5$ Bernoulli maps with and without noise: (a) shows $\langle a^2\rangle$ versus k. The time average $\langle a^2\rangle$ is computed using 1000 iterations. The power spectral densities of a_n at the positive critical values are shown in (b) for the cases without noise ($k=k_{c1}^{(0)}$, solid graph) and with noise ($k=k_{c1}$, dash-dot graph). The predicted values of critical coupling strengths and frequencies of oscillation agree with the experimental results.

values near the predicted critical values of the coupling strengths (the vertical dashed lines). Also, the power spectral density of the sequence of a_n, Fig. 1(b), shows that the frequencies of oscillation at $k=k_{c1}^{(0)}$ and $k=k_{c1}$ coincide with the predicted values $\omega_{c1}^{(0)}$ and ω_{c1} for each case. Here, and in the following examples, the power spectral densities are estimated using Welch's method [21].

In Fig. 2(a), we replot $\langle a^2\rangle$ versus k for the above described ensemble of noisy Bernoulli maps using a linear scale (dots). Also, a quadratic curve fit to the numerical data in the range $1.5 \leqslant k \leqslant 1.8$ is shown as a solid line in the same figure. We see that the fitted line agrees well with the experimental results for $k \leqslant 1.8$. Consistent with the expectation that the transition is a Hopf bifurcation (since the frequency of oscillation at transition (Fig. 1) is nonzero), $\langle a^2\rangle$ approaches zero linearly with $(k-k_{c1})$. (Close examination of the numerical results in Fig. 2(a) very near k_c shows a slight rounding of the, otherwise sharp, transition due to finite N.) Figure 2(b) shows a_{n+1} versus a_n for two values of k, one slightly past k_{c1} (coherent) and one slightly before k_{c1} (incoherent). For $k=1.45<k_{c1}=1.49$, we see that the orbit points appear as a cloud centered at the origin as expected for the incoherent state. For $k=1.53>k_{c1}$, the orbit points appear as a loop encircling the origin. As expected, at each step n points in the ring, on average, advance in angle by almost

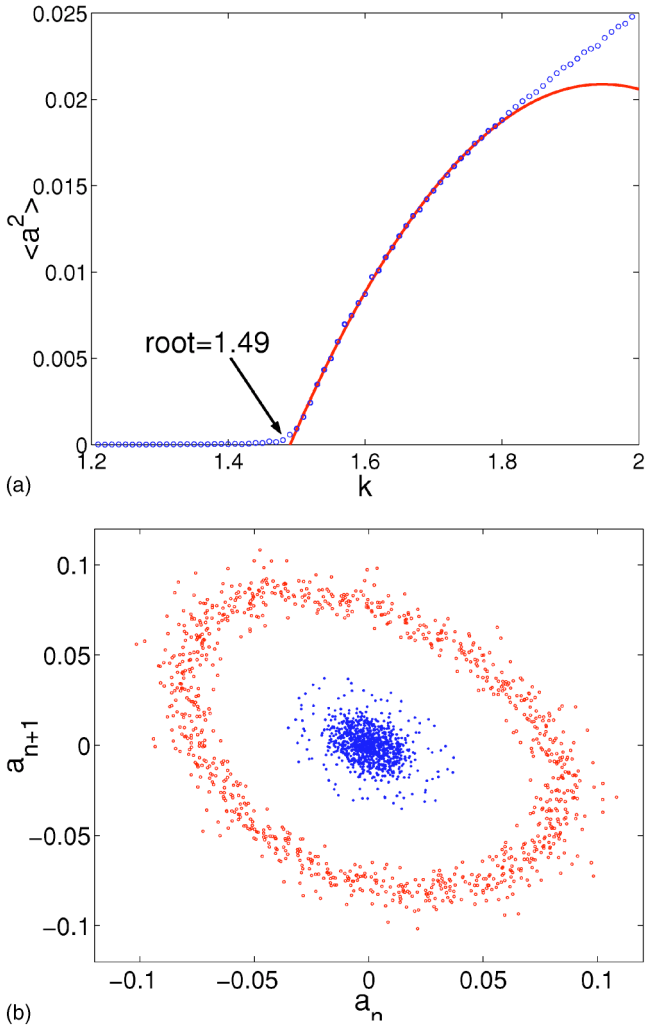

FIG. 2. Linear scale plot of $\langle a^2\rangle$ and orbits of a_n for an ensemble of 10^5 noisy Bernoulli maps: (a) shows $\langle a^2\rangle$ vs k (dots) and a quadratic curve fit (solid line) to the data in the range $1.5 \leqslant k \leqslant 1.8$. (b) shows orbits of a_n for $k=1.53 > k_{c1} \approx 1.49$ (points in halo about origin) and $k=1.45 < k_{c1}$ (points clustered near origin). $\langle a^2\rangle$ approaches zero linearly and the orbits encircle the origin consistent with a Hopf bifurcation.

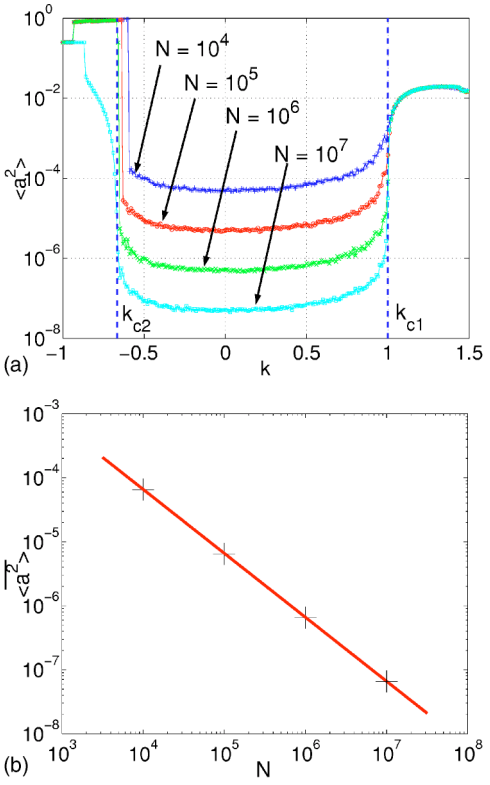

FIG. 3. Results for ensembles of $N=10^4, 10^5, 10^6, 10^7$ Bernoulli maps: (a) shows vs k. (b) shows $\langle \overline{a^2}\rangle$ vs N. Within the incoherent state $\langle a^2\rangle$ varies as N^{-1}.

ω_{c1} radians. (A plot similar to that in Fig. 2(b) appears in Ref. [19] for the noiseless case, $\sigma=0$.)

Figure 3 demonstrates the effect of varying the ensemble size N. Figure 3(a) shows results for our coupled noiseless Bernoulli map example for $N=10^4, 10^5, 10^6$, and 10^7. We note that these graphs differ appreciably only in the range $k_{c2}^{(0)} < k < k_{c1}^{(0)}$ corresponding to the incoherent state. Figure 3(b) shows the values of $\langle a^2\rangle$ averaged over the range, $(k_{c2}^{(0)} + 0.2) \leqslant k \leqslant (k_{c1}^{(0)} - 0.2)$, that is within the incoherent region (we denote this average $\langle \overline{a^2}\rangle$), versus N on a log-log plot. Also shown in Fig. 3(b) is a straight line of slope −1. We see that, similar to what is expected for a sum of random variables, a scaling of $\langle \overline{a^2}\rangle$ as N^{-1} is consistent with the data. The behavior seen in Fig. 3 is also seen for all our other examples (except for that in Sec. III C). Regarding Fig. 1(b), we also note that, as the ensemble size is increased, the spectral power not at ω_c decreases, and the spectral peak at ω_c becomes sharper, consistent with the spectrum approaching a δ function at $\omega=\omega_c$ as $N \to \infty$.

Remark. In the supercritical Hopf bifurcation of a discrete time system, the resulting stable orbit lies on a closed curve bifurcating off the basic periodic orbit that was stable before the bifurcation (in our case, the incoherent state, which has period one). On this curve, the orbit can be either periodic (consisting of a finite number of discrete points) or quasiperiodic [filling out the curve, as in Fig. 2(b)]. Generically, $\omega_c/2\pi$ will be irrational, and, for most (in the Lebesgue sense) $(k-k_c)$ values near zero, the orbit will be quasiperiodic, although there is an open dense set of values of $(k-k_c)$ for which there is an attracting periodic orbit. We note that, in our case, due to finite N, the bifurcation is noisy, and this can wash out small windows of periodic behavior.

B. A heterogeneous ensemble of modified Bernoulli maps

The preceding example, coupled Bernoulli maps, is useful because it allows an analytic solution for $Q(\lambda)$ (preceding section and Ref. [19]). In more typical cases, analytical solution for $Q(\lambda)$ is not possible, and numerical techniques for calculating $Q(\lambda)$ must be formulated. Furthermore, the maps in the ensemble may not all be identical. In order to illustrate these points, our second example is an ensemble of noiseless modified Bernoulli maps depending upon a map parameter μ that is uniformly distributed in the interval $(1,2)$,

$$f_i(x) = 2x \bmod 2\pi + \mu_i \sin x, \quad \mu_i \sim U(1,2), \quad i = 1, \ldots, N,$$

$$g(x) = \sin 4x, \quad q(x) = \cos x,$$

where $U(1,2)$ is the uniform distribution over the interval $(1,2)$.

Since we do not have a closed form expression for the natural invariant density in this case, we evaluate $Q(e^{i\omega})$ numerically in the following way. First, we produce $N=10^6$ points, x_0, uniformly distributed in the interval $(0,2\pi)$ with a random number generator, and we also produce the same number of randomly chosen parameters uniformly distributed in the interval $(1,2)$. Then we evolve the uncoupled $(k=0)$ system forward in time for 3000 steps saving the values of $x^{(i)}$ for the last 31 iterations. Using these values we construct histogram approximation to the invariant density using bins of width $2\pi \times 10^{-3}$ in x. We let x_{3000} be x_{n+1} in Eq. (11). Using the saved data, we obtain $\delta^{(i)}_{n+1}/\delta^{(i)}_{n-m+1}$ [from Eq. (8)] and $g(x^{(i)}_{n-m})$, and employ Eq. (11) to obtain an approximation to Q_m for $m=0,\ldots,30$. Note that, in the incoherent state, $x^{(i)}$ for the system (1) has an invariant density resulting from the uncoupled individual maps. Thus, if the ensemble has an infinite number of maps $(N\to\infty)$, and each orbit in the ensemble is given an initial perturbation δx_0 (as in our analysis in Sec. II), then the uncoupled ensemble will eventually settle down to the invariant density after a sufficiently large number of iterations. It is, therefore, expected that for $N\to\infty$ the mean field perturbation $\langle q'(x_n)\delta x_n\rangle$ converges to zero as n increases. Hence Q_m converges to zero with increasing m in the large ensemble limit $N\to\infty$. However, due to the finite ensemble size $(N=10^6)$, our computation of Q_m does not converge to zero. What happens is that as m increases Q_m eventually becomes small; say it assumes a small value at $m=m_c$. However, as m becomes larger, our computed approximations to Q_m become inaccurate. Since $\delta^{(i)}_{n+1}/\delta^{(i)}_{n-m+1}$ on average increases exponentially with m (chaos), the individual terms in the average (11) becomes larger and larger as m increases. On the other hand, for $N\to\infty$, the average decreases with m. Thus as m increases cancellation between terms in the average must become more and more precise. Hence to obtain good statistics for Q_m demands exponentially larger and larger ensemble size N as m increases. Thus for any finite N we expect our numerical computation of Q_m to breakdown as m increases.

We plot six numerical approximations to Q_m with different randomly chosen initial conditions in Fig. 4(a). We see that our approximations to Q_m become small at around $m=4$ or 5, but increase after that and clearly become unequal. To obtain $Q(e^{i\omega})$, we set Q_m to be zero for $m\geqslant 5$ and take the average over our six approximations. The real and imaginary parts of the resulting approximation to $Q(e^{i\omega})$ are shown in Fig. 4(b). [When the imaginary part of $Q(e^{i\omega})$ crosses zero, the real part has a maximum or minimum near these crossing points.] The greatest positive $Q(e^{i\omega})$ at a crossing point and the smallest negative $Q(e^{i\omega})$ at a crossing point are the reciprocals of the positive and negative critical coupling strengths respectively. In this example, the imaginary part of $Q(e^{i\omega})$ crosses zero four times in the plotted range. We label three of these zeros ω_{c2}, ω_{c11}, and ω_{c12}. The positive values of $Q(e^{i\omega})$ at $\omega_{c11}\approx 0.37\pi$ and $\omega_{c12}\approx\pi$ are close to each other, although the value at ω_{c12} is larger. From the real part of $Q(e^{i\omega})$, we obtain critical coupling strengths, $k_{c2}\approx -1.24$ and $k_{c12}\approx 2.48$ corresponding to ω_{c2} and ω_{c12}.

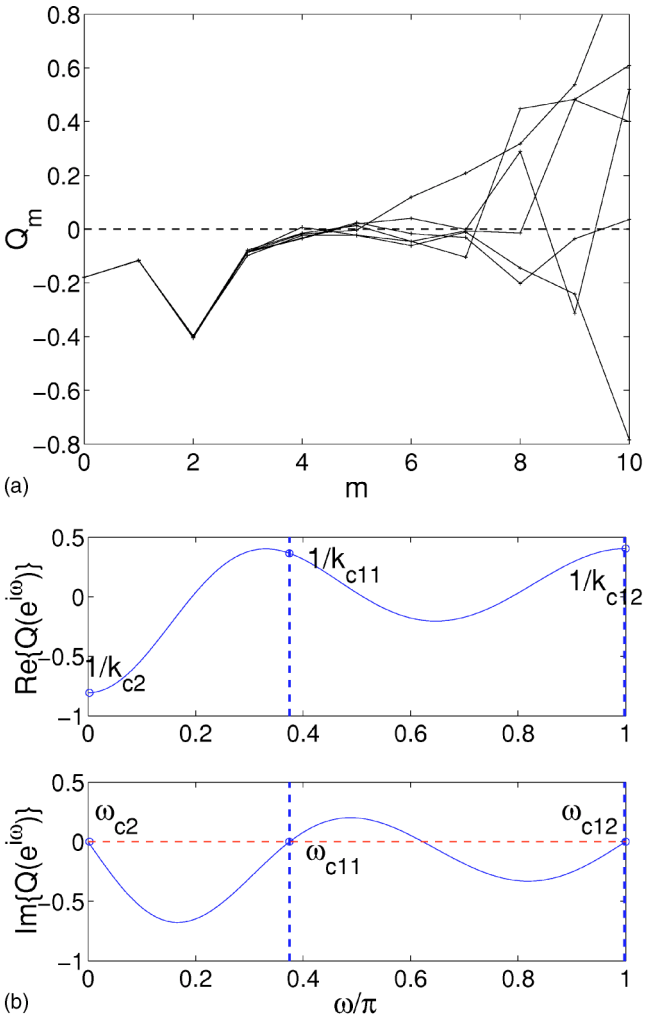

FIG. 4. $Q(e^{i\omega})$ for an ensemble of $N=10^6$ modified Bernoulli maps with uniformly distributed parameters: (a) shows six numerical approximations to Q_m. The six approximations are near zero at $m=4,5$, but then diverge from each other due to the combined effect of chaotic dynamics and finite ensemble size. (b) shows $Q(e^{i\omega})$ evaluated by averaging the six results from (a) for $m=0-4$ and taking $Q_m=0$ for $m\geqslant 5$. The imaginary part of $Q(e^{i\omega})$ has four zero-crossing points and we label three of them and corresponding real parts of these three points. The real parts corresponding to ω_{c11} and ω_{c12} are close to each other.

Results from coupled ensembles of 10^5 and 10^6 noiseless modified Bernoulli maps are shown in Fig. 5(a) along with the critical values (vertical dashed lines) which we obtained from our numerical approximation to $Q(e^{i\omega})$. We see that k_{c12} and k_{c2} closely agree with the experimental results. Figure 5(b) shows the power spectral density of a_n for $k=k_{c12}=2.48$; we note that peaks are present both at ω_{c11} (vertical dashed line) and at ω_{c12}, and that the peak at ω_{c11} is, in fact, larger, even though k_{c12} is less than $1/Q(e^{i\omega_{c11}})$.

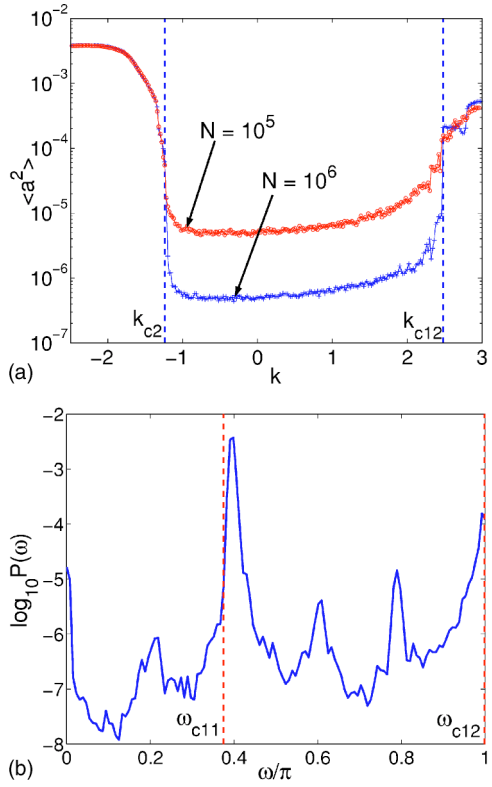

FIG. 5. Results for ensembles of $N=10^5, 10^6$ modified Bernoulli maps with uniformly distributed parameters: (a) shows $\langle a^2 \rangle$ vs k, (b) is the power spectral density of a_n at $k=2.48 \approx k_{c1}$.

C. An ensemble of logistic maps

Our third example is a noiseless ensemble of logistic maps with $g(x)=1$ and $q(x)=x$,

$$x_{n+1}^{(i)} = f(x_n^{(i)}) + k(\langle x_n \rangle - \langle x \rangle_*), \quad i = 1, \ldots, N,$$

$$f(x_n^{(i)}) = \mu x_n^{(i)}(1 - x_n^{(i)}), \tag{17}$$

where all maps have identical parameters ($\mu_i = \mu = 3.9, i = 1, \ldots, N$). In this case, we were not able to obtain useful results by use of Eq. (10). We include this example mainly to illustrate that numerical implementation of Eq. (10) can sometimes be problematic, and to speculate on why that might be the case.

In this example, we again do not have a closed form expression for the invariant density of an uncoupled map. Hence, we attempted to evaluate Q_m numerically using Eqs. (8) and (11) which in this case is simply

$$Q_m = \left\langle \frac{\delta_{n+1}}{\delta_{n-m+1}} \right\rangle. \tag{18}$$

In Fig. 6, using $N=10^9$, we plot five approximations to Q_m up to $m=35$ obtained using different random initial conditions (as in Sec. III B). We see that the five approximations stay close to each other up to $m=28$ without converging to zero. Past $m=28$, they diverge from each other. Our numerical approximations to Q_m do not converge to zero before diverging from each other, and we thus cannot predict the

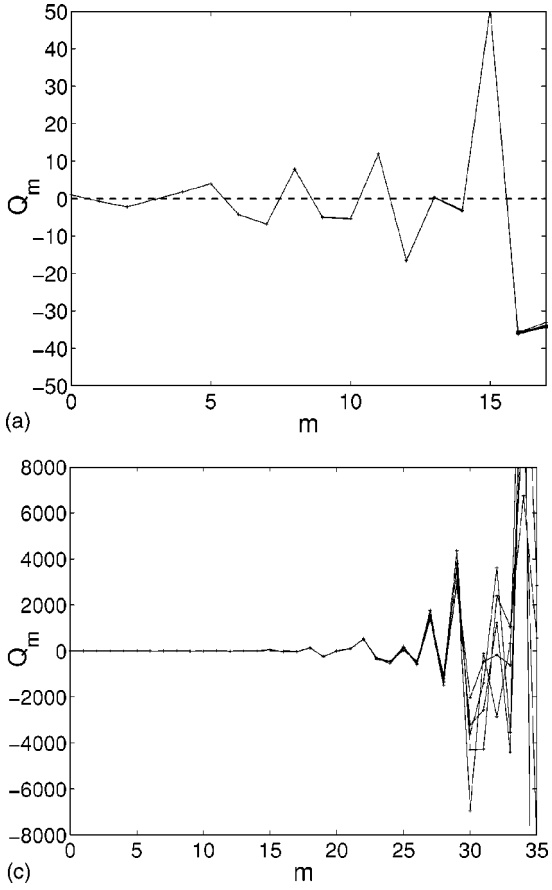

FIG. 6. Q_m for an ensemble of $N=10^9$ logistic maps with parameter $\mu=3.9$: (a) shows Q_m up to $m=17$ and (b) shows Q_m plotted up to $m=35$. We see that our approximations do not converge to small values before diverging from each other.

critical coupling strength from the theory. Since it is impractical for us to increase N further we cannot proceed further. Indeed, since Fig. 6 indicates growing oscillations of Q_m with increasing m, it is questionable that increase of N would solve the problem.

Note that the logistic map has dense periodic windows in the chaotic parameter range and that the natural invariant density $\rho(x)$ of the logistic map for typical chaotic parameter values has a dense countable set of x values at which $\rho(x)$ is infinite [22]. We speculate that this could be the root of our problem in applying Eq. (10) (see the Appendix B). In particular, both of these features call the application of the perturbation theory used in Sec. II into question.

In addition, we find that the behavior found for this example is qualitatively different from the behavior found for the examples in Secs. III A and III B. In particular, Fig. 7 shows $\langle a^2 \rangle$ versus k for $N=10^4, 10^5, 10^6$, and 10^7. We see that, unlike Fig. 3(a), the N dependence is confined to a very small region near $k=0$, and this confinement becomes narrower as N increases. Thus, if there are critical values $k_{c1}>0$ and $k_{c2}<0$, bounding an incoherent state in $k_{c2}<k<k_{c1}$, these values have very small magnitude. Another possibility (which we suspect might be the case) is that there may be no incoherent state, except at $k=0$, and that, as soon as k is nonzero, coherent behavior arises discontinuously. Such a

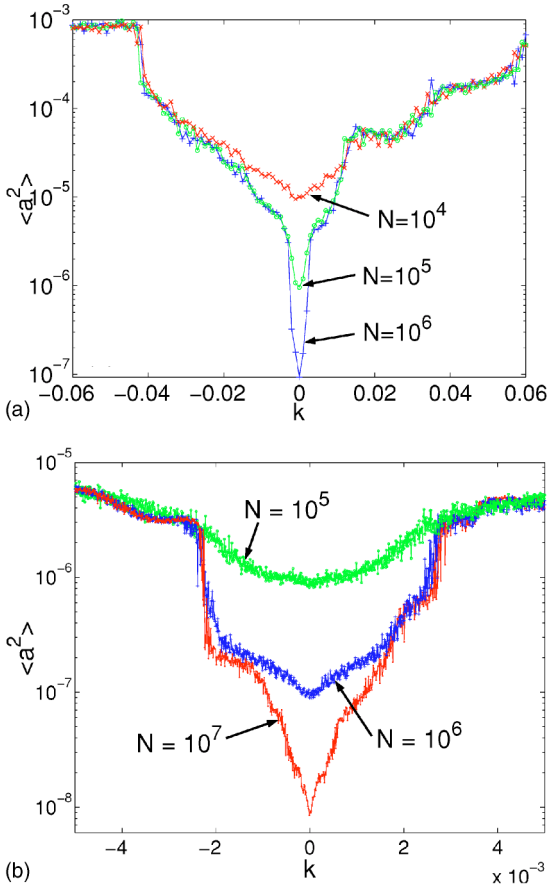

FIG. 7. $\langle a^2 \rangle$ vs k for ensembles of logistic maps: Data for ensembles of sizes $N=10^4, 10^5, 10^6$ are shown in (a). We plot $\langle a^2 \rangle$ for ensembles of $N=10^5, 10^6, 10^7$ logistic maps versus k in a narrower range of k in (b). We see that the N dependence is confined to a very small region near $k=0$ and that, as N increases, the confined region becomes narrower.

situation would be outside the scope of our perturbation theory.

D. An ensemble of logistic maps with noise

In our forth example, we consider the case studied in the preceding section, but with noise added. As mentioned in Sec. II, adding noise makes the orbit density smooth and may eliminate small periodic windows [20]. Hence, we can expect that the confinement of N dependence of $\langle a^2 \rangle$ shown in Fig. 7 will be widen and we confirmed this dependence by numerical experiments. Also, we find that the noise promotes convergence of Q_m, and that application of Eq. (10) now yields accurate and useful results. We consider Eqs. (1) with $f(x)=3.9x(1-x)$, $g(x)=1$, $q(x)=x$, and $w_n^{(i)}$ normally distributed with variance $\sigma^2=10^{-4}$ (see Sec. II). Note that $x_{n+1}^{(i)}$ in Eqs. (1) could fall outside the basin of attraction of the map $(0<x<1)$ because of the noise $w_{n+1}^{(i)}$ (the coupling term is on the order of 10^{-4} near the incoherent state with $N=10^5$ noisy logistic maps). To prevent any variable from escaping the basin, we replace $x_{n+1}^{(i)}$ by $x_{n+1}^{(i)}$ mod 1, if it falls outside the basin.

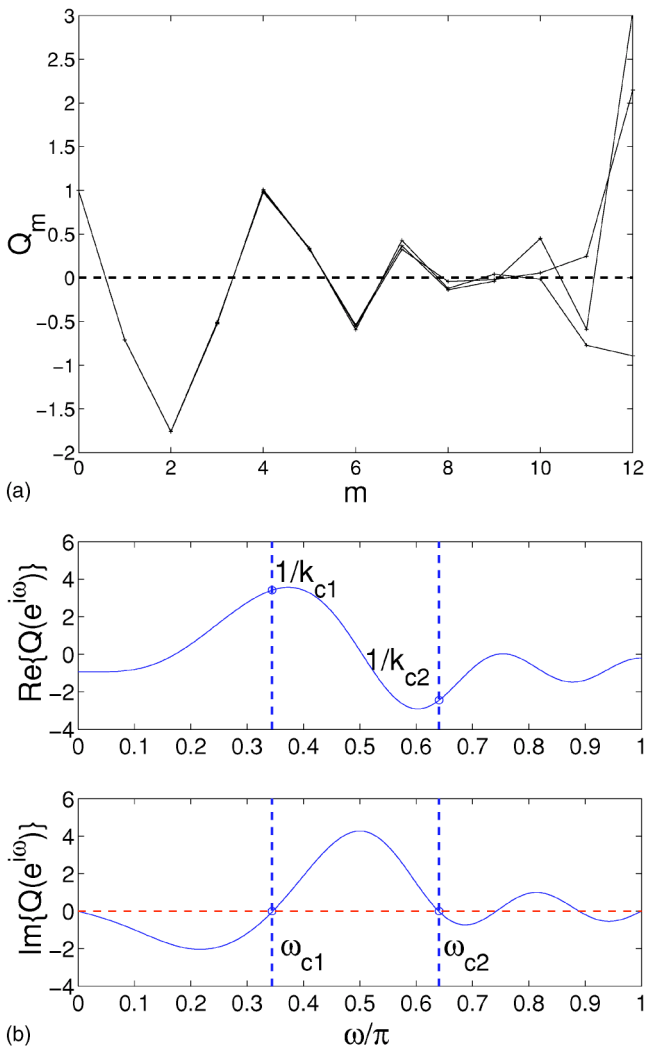

FIG. 8. $Q(e^{i\omega})$ for an ensemble of $N=10^6$ noisy logistic maps with parameter $\mu=3.9$ and normally distributed noise: (a) shows three numerical approximations to Q_m. The three approximations are near zero at $m=8,9$, but then diverge from each other. (b) shows $Q(e^{i\omega})$ evaluated from (a) assuming that $Q_m=0$ after $m=8$.

Again we do not have a closed form expression for the orbit density, and hence we rely on a numerical approximation to Q_m to obtain $Q(e^{i\omega})$. Three approximations to Q_m for different random number seeds are shown in Fig. 8(a). These three plots show good agreement with each other up to $m=9$, where they assume small values. $Q(e^{i\omega})$ derived from one of these approximations with Q_m set to zero for $m \geqslant 9$ is shown in Fig. 8(b). Using the data in Fig. 8(b), we predict that the critical values of the coupling coefficient will be $k_{c1} \approx 0.29$ and $k_{c2} \approx -0.39$, and that the corresponding frequencies of oscillation at the onset of coherence will be $\omega_{c1} \approx 0.34\pi$ and $\omega_{c2} \approx 0.64\pi$.

In Fig. 9(a) we plot the time average of the square of the mean field a_n for ensembles of 10^4 and 10^5 noisy logistic maps, $\langle a^2 \rangle$, and the predicted values of the critical coupling strengths (vertical dashed lines), k_{c1} and k_{c2}. We replot $\langle a^2 \rangle$ using a linear scale in Fig. 9(b) (dots). Also shown in Fig. 9(b) as a solid line is a quadratic curve fit to the numerical

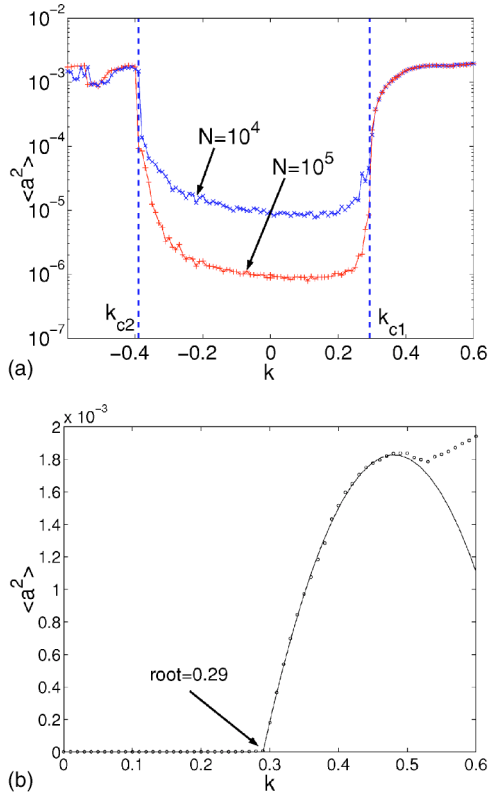

FIG. 9. Experimental results for an ensemble of $N=10^4,10^5$ noisy logistic maps with parameter $\mu=3.9$ and normally distributed noise: (a) shows a semilogarithmic plot of $\langle a^2\rangle$ vs k, and (b) shows $\langle a^2\rangle$ (dots) and a quadratic curve fit to the numerical data in the range $0.29\leqslant k\leqslant 0.44$ (solid line) for $N=10^5$.

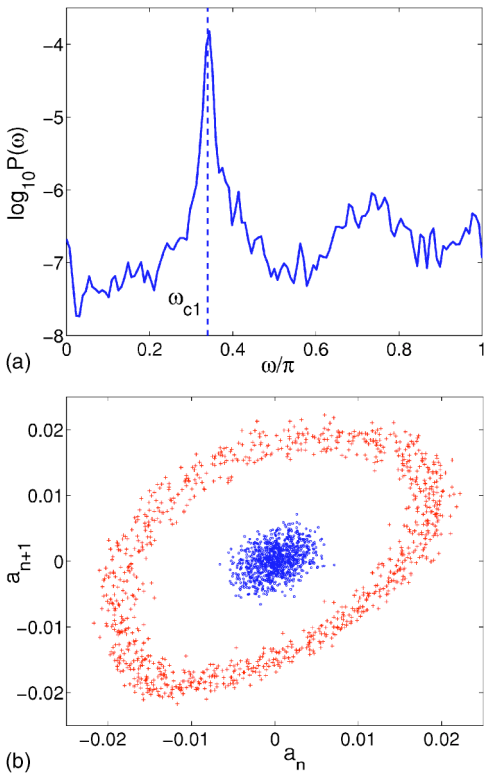

FIG. 10. Power spectral density and orbits of a_n for $N=10^4$: The frequency of oscillation and the power spectral density of a_n at $k=k_{c1}$ are plotted in (a). (b) shows orbits of a_n for $k=0.30>k_{c1}\approx 0.29$ (points in halo about origin) and $k=0.28<k_{c1}$ (points clustered near origin).

data in the range $0.29\leqslant k\leqslant 0.44$ which agrees well with the experimental results for $k\leqslant 0.51$. Extrapolating the fitted quadratic curve to $\langle a^2\rangle=0$, we obtain an accurate estimate of the critical value of the coupling strength, $k\approx 0.29$, confirming the theoretical prediction. From Fig. 9(b) we see that $\langle a^2\rangle$ approaches zero linearly with $(k-k_{c1})$ consistent with a Hopf bifurcation $(\omega_{c1}\neq 0)$.

The frequency of oscillation at $k=k_{c1}$ obtained from $Q(e^{i\omega})$ is shown in Fig. 10(a) as a vertical dashed line, along with the power spectral density of a_n. The dominant frequency of the spectrum agrees with the frequency predicted by our analysis. Figures 10(b) shows a_{n+1} versus a_n for two values of k, one just past k_{c1} (coherent) and one just before k_{c1} (incoherent). For $k=0.28<k_{c1}=0.29$, we see that the orbit points appear as a cloud centered at the origin. For $k=0.30>k_{c1}$, the orbit points appear as a loop encircling the origin (at the frequency ω_{c1}).

E. A heterogeneous ensemble of logistic maps

In our fifth example, as in Sec. III C, we again consider a noiseless ensemble of logistic maps (17), but now with the map parameter, μ, uniformly distributed in the interval $(3.88,3.96)$. We find that the introduction of parameter spread appears to have a regularizing effect and, for this noiseless case, we now obtain results in agreement with our perturbation theory. A similar regularizing effect has been observed by Shibata and Kaneko [17].

Figure 11(a) shows six approximations to Q_m for different random number seeds. They agree well with each other up to $m=12$, where they assume small values. $Q(e^{i\omega})$ shown in Fig. 11(b) is derived from one of these approximations with Q_m set to zero for $m\geqslant 12$. From Fig. 11(b) we predict that the critical coupling strengths will be $k_{c1}\approx 0.24$ and $k_{c2}\approx -0.13$, and that the corresponding frequencies of oscillation at the onset of coherence will be $\omega_{c1}\approx 0.37\pi$ and $\omega_{c2}\approx 0.60\pi$.

In Fig. 12(a) we plot the time average of the square of the mean field for noiseless ensembles of $10^4,10^5$, and 10^6 logistic maps with the parameter, μ, uniformly distributed in the interval $(3.88,3.96)$. The power spectral density of a_n at $k\approx k_{c1}$ is shown in Fig. 12(b). We see that the predicted values agree well with the numerical experiments. Note that the peak around $\omega=0.74\pi$ is also expected from the data in Fig. 11(b). The real part of $Q(e^{i\omega})$ at $\omega\approx 0.74\pi$, where the imaginary part crosses zero, has a value comparable with that at $k=k_{c1}$.

IV. EXAMPLES: TWO-DIMENSIONAL MAPS

In this section we examine globally coupled multidimensional systems for which, analogous to the system (1), the considered system is

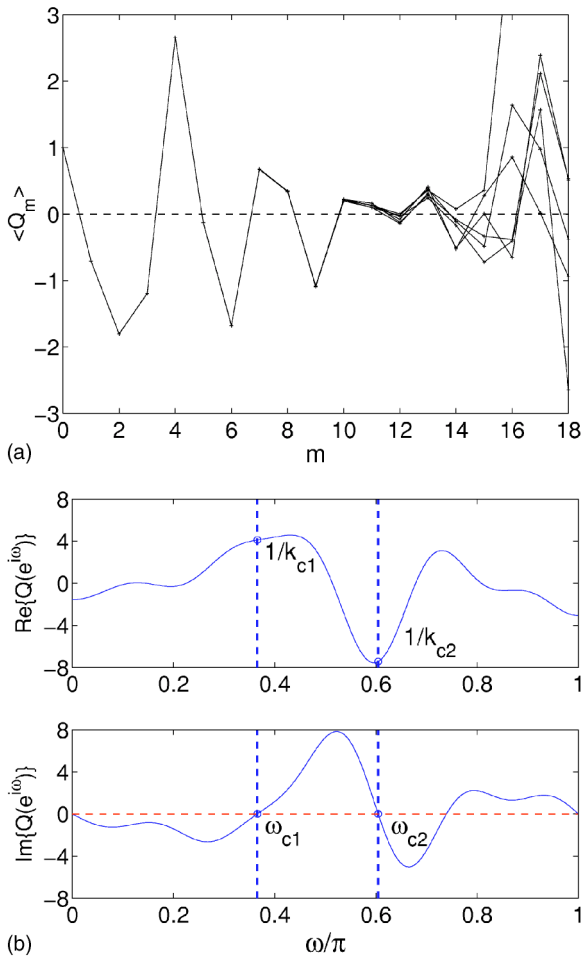

FIG. 11. $Q(e^{i\omega})$ for a noiseless ensemble of $N=10^9$ logistic maps with parameter μ uniformly distributed in the interval (3.88,3.96): (a) shows three numerical approximations to Q_m. The three approximations are near zero at $m=12$, but then diverge from each other. (b) shows $Q(e^{i\omega})$ evaluated from (a) assuming that $Q_m=0$ after $m=12$.

$$\mathbf{x}_{n+1}^{(i)} = \mathbf{f}(\mathbf{x}_n^{(i)}) + \mathbf{w}_n^{(i)} + \mathbb{G}(\mathbf{x}_n)\mathbb{K}(\langle \mathbf{q}(\mathbf{x}_n)\rangle - \langle \mathbf{q}(\mathbf{x})\rangle_*),$$
$$i = 1, \ldots, N,$$

where $\mathbf{x}_n=[x_{1,n}x_{2,n}\ldots x_{r,n}]^{\mathrm{T}}$, r is the dimension of a map, $\mathbb{K}$ is the coupling matrix, $\mathbb{G}(\mathbf{x}_n)$ is a matrix function, and $\mathbf{q}(\mathbf{x}_n)$ is a vector function of $\mathbf{x}_n$. Here, $\mathbf{w}_n^{(i)}$ is random noise where $E[\mathbf{w}_n^{(i)}]=0$, $E[\mathbf{w}_n^{(i)}\mathbf{w}_k^{(j)\mathrm{T}}]=\Sigma\delta_{ij}\delta_{nk}$, Σ is the covariance matrix, and we assume that the noise at each iterate is identically distributed and that $\mathbf{x}_n$ and $\mathbf{w}_n$ are independent.

Let $\mathbf{Df}(\mathbf{x})=\partial\mathbf{f}(\mathbf{x})/\partial\mathbf{x}$ and

$$\mathbb{M}(n,p) = \begin{cases} \mathbf{Df}(\mathbf{x}_{n-1})\mathbf{Df}(\mathbf{x}_{n-2})\cdots\mathbf{Df}(\mathbf{x}_p), & n \geqslant p+1, \\ \mathbb{I}, & n = p \end{cases}$$

where $\mathbb{I}$ is the identity matrix. Then proceeding as in Sec. II, we assume that the mean of the perturbation $\delta\mathbf{x}$ grows exponentially with n, $\langle \mathbf{Dq}(\mathbf{x}_n)\delta\mathbf{x}_n\rangle = \mathbf{v}\lambda^n$, where $\mathbf{v}=\langle \mathbf{Dq}(\mathbf{x}_0)\delta\mathbf{x}_0\rangle$. Letting $n\to\infty$, assuming convergence of the summation, and setting $m=n-p$, we obtain

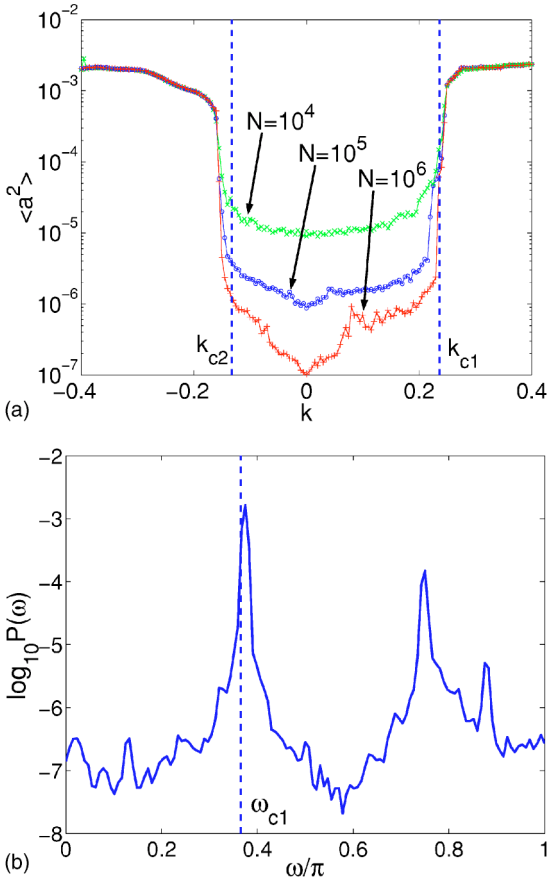

FIG. 12. Experimental results for a noiseless ensemble of $N=10^4, 10^5, 10^6$ logistic maps with parameter μ uniformly distributed in the interval (3.88,3.96): (a) shows $\langle a^2\rangle$ vs k, and (b) shows the power spectral density of a_n at $k=0.24\approx k_{c1}$ for $N=10^6$.

$$(\mathbb{I} - \mathbb{Q}(\lambda)\mathbb{K})\mathbf{v} = 0.$$

where

$$\mathbb{Q}(\lambda) = \sum_{m=1}^{\infty} \mathbb{Q}_m/\lambda^m,$$

$$\mathbb{Q}_m = \langle \mathbf{Dq}(\mathbf{x}_n)\mathbb{M}(n,n-m+1)\mathbb{G}(\mathbf{x}_{n-m})\rangle, \tag{19}$$

which yields

$$\det(\mathbb{I} - \mathbb{Q}(\lambda)\mathbb{K}) = 0. \tag{20}$$

By setting $\lambda=e^{i\omega}$ in Eq. (20), we can determine the critical coupling strength and the frequency of oscillation (see Sec. II).

We now illustrate Eq. (20) by application to an ensemble of globally coupled two-dimensional maps. In particular, we take $\mathbf{f}(\mathbf{x})$ to be the cat map,

$$\mathbf{f}(\mathbf{x}) = \begin{bmatrix} x+y \\ x+2y \end{bmatrix} \bmod 2\pi, \quad \mathbf{q}(\mathbf{x}) = \begin{bmatrix} \cos x \\ 0 \end{bmatrix},$$

$$\mathbb{G}(\mathbf{x}) = \begin{bmatrix} \sin(2x+3y) & 0 \\ 0 & 0 \end{bmatrix}, \quad \mathbb{K} = \begin{bmatrix} k & 0 \\ 0 & 0 \end{bmatrix}, \tag{21}$$

where $\mathbf{x}_n = [x_n y_n]^{\mathrm{T}}$. For the noise, we choose

$$E[\mathbf{w}_n^{(i)}] = 0, \quad E[\mathbf{w}_n^{(i)} \mathbf{w}_k^{(j)\mathrm{T}}] = \begin{bmatrix} \sigma^2 & 0 \\ 0 & \sigma^2 \end{bmatrix} \delta_{ij} \delta_{nk},$$

where $\mathbf{w}_n^{(i)} = [w_{x,n}^{(i)} w_{y,n}^{(i)}]^{\mathrm{T}}$. We denote the element at the kth row and the lth column of a matrix A by $[A]_{kl}$. Then, after plugging Eqs. (21) into Eqs. (19), we obtain

$$[\mathbb{Q}_n(\lambda)]_{11} = -\sum_{p=0}^{n-1} \langle \sin x_n \sin(2x_p + 3y_p) \rangle \frac{[\mathbb{M}(n,p+1)]_{11}}{\lambda^{n-p}}$$

$$= -\frac{1}{2\lambda^2} \langle \cos(w_{x,n} + w_{x,n-1} + w_{y,n-1}) \rangle.$$

The second equality results from noting that, since the measure generated by orbits of the uncoupled noisy cat maps is uniform in $0 \leqslant x \leqslant 2\pi, 0 \leqslant y \leqslant 2\pi$, all terms in the summation are zero except for $p = n-2$. For normally distributed noise, $[\mathbb{Q}_n(\lambda)]_{11} = -(2\lambda^2)^{-1} \exp(-3\sigma^2/2)$. From the condition (20), we obtain

$$\frac{1}{k} = -\frac{e^{-3\sigma^2/2}}{2e^{2i\omega}},$$

which yields the critical values $k_{c1} = 2e^{3\sigma^2/2}$ at $\omega_{c1} = \pi/2$ and $k_{c2} = -2e^{3\sigma^2/2}$ at $\omega_{c2} = 0$.

Figure 13 shows results of numerical experiments for this system without noise and with noise ($\sigma^2 = 0.16$). Without noise, the critical values are $k_{c1}^{(0)} = 2$ at $\omega_{c1}^{(0)} = \pi/2$ and $k_{c2}^{(0)} = -2$ at $\omega_{c2}^{(0)} = 0$. With noise, the critical values are $k_{c1} \approx 2.54$ at $\omega_{c2} = \pi/2$ and $k_{c2} \approx -2.54$ at $\omega_{c2} = 0$. In Fig. 13(a), we see that the transition occurs near the predicted critical values for each case. Also, Fig. 13(b) shows that the predicted frequencies of oscillation at $k = k_{c1}^{(0)}$ and $k = k_{c1}$ (which is $\pi/2$ in both cases) match the peaks of the power spectral densities of a_n for each k.

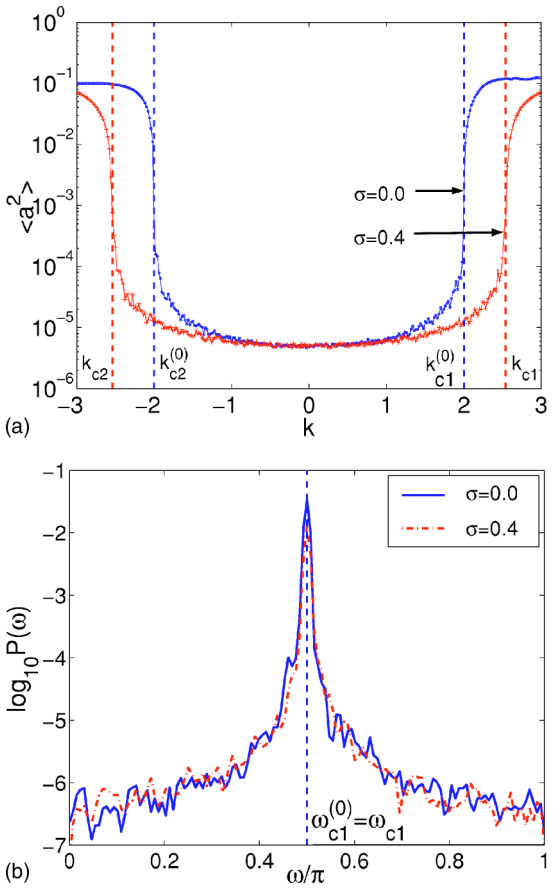

FIG. 13. Experimental results for an ensemble of $N = 10^5$ cat maps with and without noise: (a) shows k vs $\langle a^2 \rangle$ for the cases with noise and without noise. (b) show the power spectral densities of a_n at the positive critical values for the cases without noise ($k = k_{c1}^{(0)}$, solid graph) and with noise ($k = k_{c1}$, dash-dot graph).

V. CONCLUSION

A large class of globally coupled systems of chaotic maps experience a transition from incoherence to coherence at critical values of a coupling coefficient. We have shown that these critical values can be determined from a perturbation method, and we apply our method to ensembles of homogeneous chaotic maps, ensembles of chaotic maps with distributed parameters, and ensembles of chaotic maps with noise. We have shown that numerical approximations to $Q(e^{i\omega})$ can be sufficiently accurate to yield good predictions for the transition, provided that a large enough number of elements is used in obtaining the approximations.

In our numerical experiments we obtained good agreement with our theory for ensembles of a large number of noisy Bernoulli maps, for a noiseless system of modified Bernoulli maps with distributed parameters, for noisy logistic maps, and for a noisy system of cat maps (a two-dimensional example). However, we did not obtain useful results from our analysis when we attempted to apply it to an ensemble of identical noise-free logistic maps. We speculate that this may be due to the facts that the natural invariant density $\rho(x)$ of the logistic map, in common with other generic nonhyperbolic maps, has a dense countable set of x values at which $\rho(x)$ is infinite and that the map is structurally unstable (it has a dense set of periodic windows in its chaotic parameter range). Structural instability, for example, implies that a small perturbation can result in totally different dynamics, and hence application of a perturbation method may be questionable. On the other hand, we have found that either noise or parameter spread appears to restore the validity of the perturbation theory approach. It would be worthwhile to further investigate noiseless ensembles of smooth maps that have a dense set of periodic windows.

ACKNOWLEDGMENTS

The authors acknowledge support from the Office of Naval Research (Physics) and the National Science of Foundation (Grant No. PHYS 0098632).

APPENDIX A: DECAY OF Q_m WITH INCREASING m

In this appendix we give a heuristic argument suggesting that, in typical cases, it is reasonable to hypothesize that, for large m, Q_m decays exponentially with increasing m. For definiteness, we consider the case of a map $x_{n+1}=f(x_n)$ of the real line, $-\infty \leqslant x \leqslant +\infty$, which has a single chaotic attractor in some bounded region of x, and we also assume that this attractor has a natural invariant measure [also called a Sinai-Ruelle-Bowen measure]. By definition the natural measure is the unique invariant measure, ν, such that, for any smooth function $s(x)$, the time average of $s(x_n)$ over an orbit is $\int s(x)d\nu$ for orbits generated by Lebesgue almost every initial condition x_0 in the basin of attractor. Recalling that $g(x)$ and $q(x)$ are smooth bounded functions, we anticipate that the decay of Q_m does not depend critically on details of these functions. Thus we consider the illustrative example of Eq. (18). Using Eq. (8) we express Eq. (18) as

$$Q_m = \langle f'(x_n)f'(x_{n-1})\cdots f'(x_{n-m+1})\rangle.$$

The average, $\langle\cdots\rangle$, is over an infinite number of initial conditions $x_0^{(i)}$ which are distributed on the attractor according to the natural invariant measure. Since the natural measure is invariant,

$$Q_m = \langle f'(x_{m-1})f'(x_{m-2})\cdots f'(x_0)\rangle = \langle \delta_m\rangle.$$

The quantity $\langle \delta_m\rangle$ has a simple geometric interpretation. Imagine that, at time $m=0$, we displace all the initial condition by the same amount dx_0. That is, we rigidly translate the natural invariant measure by an amount dx_0. Thus, at any subsequent time m, $\langle \delta_m\rangle dx_0$ is the displacement of the evolved orbits averaged over all orbits. In other words, $\langle \delta_m\rangle dx_0$ is the displacement of the centroid of the evolved measure from the centroid of the natural invariant measure. Since, by definition, the natural invariant measure is generated by the time average of Lebesgue almost any initial condition in the basin of the attractor, $\langle \delta_m\rangle$ should relax to zero as m increases. Thus, for the example (18), our hypothesis that Q_m decays exponentially, is equivalent to the hypothesis that the displaced centroid of a cloud of orbits relaxes exponentially to its equilibrium value. This is rigorously true for the case of hyperbolic attractors [23], and we also adopt it as a useful working hypothesis for the general case. We caution, however, that this hypothesis may not always be valid (see Sec. III C and Appendix B).

APPENDIX B: ORBIT DENSITIES FOR ENSEMBLES OF LOGISTIC MAPS

In this appendix, we attempt to gain understanding concerning the observed lack of convergence found for the example in Sec. III C. To do this we numerically examine how the orbit density evolves after a small perturbation from the natural time asymptotic invariant density. We evolve a large number of orbits (10^7 with $\mu=3.9$), initially uniformly distributed, forward in time for many iterates, (to approximately reach the invariant orbit density), and, by duplicating, two identical orbit distributions are created. Then, one of the orbit distributions is perturbed by adding the same small perturbation $\delta x_0=10^{-3}$ to every orbit points. We then evolve both sets of orbits forward in time and observe the orbit densities to see how the perturbed density relates to the unperturbed invariant density. We divide the interval $(0,1)$ into 1000 subintervals, count the number of orbits in each subinterval, normalize the numbers, and plot these numbers for each subinterval. This histogram procedure yields an approximation to the density with resolution 10^{-3}.

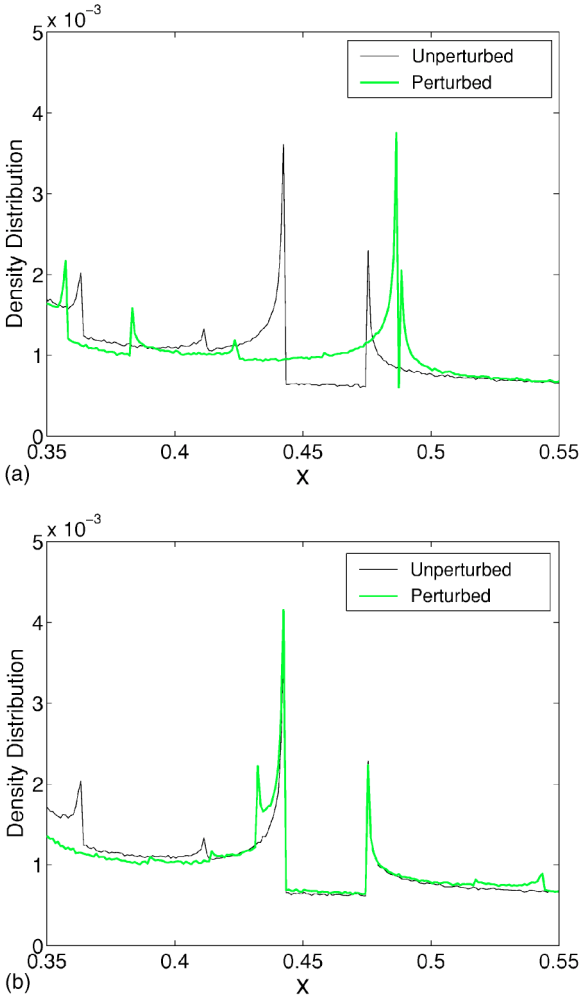

FIG. 14. The histogram approximated orbit densities in the interval $[0.35,0.55]$ for ensembles of 10^7 identical logistic maps with parameter $\mu=3.9$ with the initial perturbation $\delta x_0=10^{-3}$ (gray) and without perturbation (black): We set time t to 0 at which the perturbation is applied. (a) and (b) show the densities at $t=4$ and $t=10$, respectively.

In Fig. 14, we plot our histogram approximation of the orbit densities for the perturbed case (gray) and for the unperturbed case (black) in a small interval $0.35 \leqslant x \leqslant 0.55$. The perturbation $\delta x_0=10^{-3}$ rigidly shifts the original invariant density slightly to the right. Setting t to 0 at this moment, Figs. 14(a) and 14(b) show the orbit densities at $t=4$ and $t=10$, respectively. We find that the perturbed density is distorted significantly by around $t=8$ so that the outstanding peaks in the perturbed density do not match those in the

unperturbed (i.e., invariant) density. Thus the small perturbation δx_0 in the orbit location points leads to large perturbations in the absolute value of the histogram approximation of orbit density near points where the histogram approximated density has strong narrow peaks. After $t=8$, the histogram approximated perturbed density becomes closer to the histogram approximated invariant density. However, it is to be expected that as the resolution of the histogram is increased, large differences in the approximated densities would be observed out to later and later times. This is a reflection of the singular nature of the density and suggests that the perturbation theory approach is not valid.

[1] A. T. Winfree, Science **298**, 2336 (2002); S. Nadis, Nature (London) **421**, 780 (2003); S. Strogatz, *Sync: The Emerging Science of Spontaneous Order* (Hyperion, New York, 2003); Y. Kuramoto, *Chemical Oscillations, Waves and Turbulences* (Springer-Verlag, Berlin, 1984).

[2] L. Glass, Nature (London) **410**, 277 (2001); L. Glass and M. C. Mackey, *From Clocks to Chaos* (Princeton University Press, Princeton, 1988).

[3] D. C. Michaels, E. P. Matyas, and J. Jalife, Circ. Res. **61**, 704 (1987).

[4] C. M. Gray, J. Comput. Neurosci. **1**, 11 (1994); M. I. Rabinovich and H. D. I. Abarbanel, Neuroscience **87**, 5 (1998); D. H. Zanette and A. S. Mikhailov, Phys. Rev. E **58**, 872 (1998); N. F. Rulkov, Phys. Rev. Lett. **86**, 183 (2001); J. J. Hopfield and C. D. Brody, Proc. Natl. Acad. Sci. U.S.A. **98**, 1282 (2001).

[5] S. Yamaguchi, H. Isejima, T. Matsuo, R. Okura, K. Yagita, M. Kobayashi, and H. Okamura, Science **302**, 1408 (2003).

[6] S. Dane, P. G. Sorensen, and F. Hynne, Nature (London) **402**, 320 (1999).

[7] J. Buck, Q. Rev. Biol. **63**, 265 (1988); F. E. Hanson, J. F. Case, E. Buck, and J. Buck, Science **174**, 161 (1971); J. Buck and E. Buck, *ibid.* **159**, 1319 (1968).

[8] T. J. Walker, Science **166**, 891 (1969); E. Sismondo, *ibid.* **249**, 55 (1990).

[9] W. Wand, I. Z. Kiss, and J. L. Hudson, Chaos **10**, 248 (2000); I. Z. Kiss, Y. Zhai, and J. L. Hudson, Science **296**, 1676 (2002).

[10] G. Kozyreff, A. G. Vladimirov, and P. Mandel, Phys. Rev. Lett. **85**, 3809 (2000).

[11] K. Wiesenfeld, P. Colet, and S. H. Strogatz, Phys. Rev. Lett. **76**, 404 (1996).

[12] A. S. Pikovsky, M. G. Rosenblum, and J. Kurths, Europhys. Lett. **34**, 165 (1996).

[13] H. Sakaguchi, Phys. Rev. E **61**, 7212 (2000).

[14] E. Ott, P. So, E. Barreto, and T. Antonsen, Physica D **173**, 29 (2002).

[15] K. Kaneko, Phys. Rev. Lett. **65**, 1391 (1990).

[16] G. Perez and H. A. Cerdeira, Phys. Rev. A **46**, 7492 (1992); A. S. Pikovsky and J. Kurths, Phys. Rev. Lett. **72**, 1644 (1994).

[17] T. Shibata and K. Kaneko, Europhys. Lett. **38**, 417 (1997).

[18] T. Shibata and K. Kaneko, Phys. Rev. Lett. **81**, 4116 (1998); M. Cencini, M. Falcioni, D. Vergni, and A. Vulpiani, Physica D **130**, 58 (1999).

[19] D. Topaj, W. -H. Kye, and A. Pikovsky, Phys. Rev. Lett. **87**, 074101 (2001).

[20] S. Seshadri, V. Balakrishnan, and S. Lakshmibala, Phys. Rev. E **60**, 386 (1999); E. Ott and J. D. Hanson, Phys. Lett. **85A**, 20 (1981); E. Ott, E. D. Yorke, and J. A. Yorke, J. Stat. Phys. **36**, 687 (1984).

[21] P. Stoica and R. Moses, *Introduction to Spectral Analysis* (Prentice-Hall, Upper Saddle River, 1997), Chap. 2; MATLAB 6.1 RELEASE 12.1 (The MathWorks Inc., Natick, 2001).

[22] E. Ott, *Chaos in Dynamical Systems*, 2nd Ed. (Cambridge University Press, Cambridge, 2002), Chap. 2.

[23] L. -S. Young, Ann. Math. **147**, 585 (1998).